Inference of the Mass Composition of Cosmic Rays with Energies from $10^{18.5}$ to 10^{20} eV Using the Pierre Auger Observatory and Deep Learning

A. Abdul Halim,[13] P. Abreu,[71] M. Aglietta,[53,51] I. Allekotte,[1] K. Almeida Cheminant,[79,78,69] A. Almela,[7,12] R. Aloisio,[44,45] J. Alvarez-Muñiz,[77] J. Ammerman Yebra,[77] G. A. Anastasi,[57,46] L. Anchordoqui,[84] B. Andrada,[7] L. Andrade Dourado,[44,45] S. Andringa,[71] L. Apollonio,[58,48] C. Aramo,[49] P. R. Araújo Ferreira,[41] E. Arnone,[62,51] J. C. Arteaga Velázquez,[66] P. Assis,[71] G. Avila,[11] E. Avocone,[56,45] A. Bakalova,[31] F. Barbato,[44,45] A. Bartz Mocellin,[83] C. Berat,[35] M. E. Bertaina,[62,51] G. Bhatta,[69] M. Bianciotto,[62,51] P. L. Biermann,[*] V. Binet,[5] K. Bismark,[38,7] T. Bister,[78,79] J. Biteau,[36,†] J. Blazek,[31] C. Bleve,[35] J. Blümer,[40] M. Boháčová,[31] D. Boncioli,[56,45] C. Bonifazi,[8] L. Bonneau Arbeletche,[22] N. Borodai,[69] J. Brack,[‡] P. G. Brichetto Orchera,[7] F. L. Briechle,[41] A. Bueno,[76] S. Buitink,[15] M. Buscemi,[46,57] M. Büsken,[38,7] A. Bwembya,[78,79] K. S. Caballero-Mora,[65] S. Cabana-Freire,[77] L. Caccianiga,[58,48] F. Campuzano,[6] R. Caruso,[57,46] A. Castellina,[53,51] F. Catalani,[19] G. Cataldi,[47] L. Cazon,[77] M. Cerda,[10] B. Čermáková,[40] A. Cermenati,[44,45] J. A. Chinellato,[22] J. Chudoba,[31] L. Chytka,[32] R. W. Clay,[13] A. C. Cobos Cerutti,[6] R. Colalillo,[59,49] M. R. Coluccia,[47] R. Conceição,[71] A. Condorelli,[36] G. Consolati,[48,54] M. Conte,[55,47] F. Convenga,[56,45] D. Correia dos Santos,[27] P. J. Costa,[71] C. E. Covault,[82] M. Cristinziani,[43] C. S. Cruz Sanchez,[3] S. Dasso,[4,2] K. Daumiller,[40] B. R. Dawson,[13] R. M. de Almeida,[27] B. de Errico,[27] J. de Jesús,[7,40] S. J. de Jong,[78,79] J. R. T. de Mello Neto,[27] I. De Mitri,[44,45] J. de Oliveira,[18] D. de Oliveira Franco,[47] F. de Palma,[55,47] V. de Souza,[20] E. De Vito,[55,47] A. Del Popolo,[57,46] O. Deligny,[33] N. Denner,[31] L. Deval,[40,7] A. di Matteo,[51] J. A. do,[13,68] M. Dobre,[72] C. Dobrigkeit,[22] J. C. D'Olivo,[67] L. M. Domingues Mendes,[16,71] Q. Dorosti,[43] J. C. dos Anjos,[16] R. C. dos Anjos,[26] J. Ebr,[31] F. Ellwanger,[40] M. Emam,[78,79] R. Engel,[38,40] I. Epicoco,[55,47] M. Erdmann,[41] A. Etchegoyen,[7,12] C. Evoli,[44,45] H. Falcke,[78,80,79] G. Farrar,[86] A. C. Fauth,[22] T. Fehler,[43] F. Feldbusch,[39] F. Fenu,[40,§] A. Fernandes,[71] B. Fick,[85] J. M. Figueira,[7] P. Filip,[38,7] A. Filipčič,[75,74] T. Fitoussi,[40] B. Flaggs,[88] T. Fodran,[78] T. Fujii,[87,‖] A. Fuster,[7,12] C. Galea,[78] B. García,[6] C. Gaudu,[37] A. Gherghel-Lascu,[72] P. L. Ghia,[33] U. Giaccari,[47] J. Glombitza,[41,¶] F. Gobbi,[10] F. Gollan,[7] G. Golup,[1] M. Gómez Berisso,[1] P. F. Gómez Vitale,[11] J. P. Gongora,[11] J. M. González,[1] N. González,[7] D. Góra,[69] A. Gorgi,[53,51] M. Gottowik,[40] F. Guarino,[59,49] G. P. Guedes,[23] E. Guido,[43] L. Gülzow,[40] S. Hahn,[38] P. Hamal,[31] M. R. Hampel,[7] P. Hansen,[3] D. Harari,[1] V. M. Harvey,[13] A. Haungs,[40] T. Hebbeker,[41] C. Hojvat,[**] J. R. Hörandel,[78,79] P. Horvath,[32] M. Hrabovský,[32] T. Huege,[40,15] A. Insolia,[57,46] P. G. Isar,[73] P. Janecek,[31] V. Jilek,[31] J. A. Johnsen,[83] J. Jurysek,[31] K.-H. Kampert,[37] B. Keilhauer,[40] A. Khakurdikar,[78] V. V. Kizakke Covilakam,[7,40] H. O. Klages,[40] M. Kleifges,[39] F. Knapp,[38] J. Köhler,[40] F. Krieger,[41] N. Kunka,[39] B. L. Lago,[17] N. Langner,[41] M. A. Leigui de Oliveira,[25] Y. Lema-Capeans,[77] A. Letessier-Selvon,[34] I. Lhenry-Yvon,[33] L. Lopes,[71] L. Lu,[89] Q. Luce,[38] J. P. Lundquist,[74] A. Machado Payeras,[22] M. Majercakova,[31] D. Mandat,[31] B. C. Manning,[13] P. Mantsch,[**] F. M. Mariani,[58,48] A. G. Mariazzi,[3] I. C. Mariş,[14] G. Marsella,[60,46] D. Martello,[55,47] S. Martinelli,[40,7] O. Martínez Bravo,[63] M. A. Martins,[77] H.-J. Mathes,[40] J. Matthews,[††] G. Matthiae,[61,50] E. Mayotte,[83] S. Mayotte,[83] P. O. Mazur,[**] G. Medina-Tanco,[67] J. Meinert,[37] D. Melo,[7] A. Menshikov,[39] C. Merx,[40] S. Michal,[31] M. I. Micheletti,[5] L. Miramonti,[58,48] S. Mollerach,[1] F. Montanet,[35] L. Morejon,[37] K. Mulrey,[78,79] R. Mussa,[51] W. M. Namasaka,[37] S. Negi,[31] L. Nellen,[67] K. Nguyen,[85] G. Nicora,[9] M. Niechciol,[43] D. Nitz,[85] D. Nosek,[30] V. Novotny,[30] L. Nožka,[32] A. Nucita,[55,47] L. A. Núñez,[29] C. Oliveira,[20] M. Palatka,[31] J. Pallotta,[9] S. Panja,[31] G. Parente,[77] T. Paulsen,[37] J. Pawlowsky,[37] M. Pech,[31] J. Pękala,[69] R. Pelayo,[64] V. Pelgrims,[14] L. A. S. Pereira,[24] E. E. Pereira Martins,[38,7] C. Pérez Bertolli,[7,40] L. Perrone,[55,47] S. Petrera,[44,45] C. Petrucci,[56] T. Pierog,[40] M. Pimenta,[71] M. Platino,[7] B. Pont,[78] M. Pothast,[79,78] M. Pourmohammad Shahvar,[60,46] P. Privitera,[87] M. Prouza,[31] S. Querchfeld,[37] J. Rautenberg,[37] D. Ravignani,[7] J. V. Reginatto Akim,[22] M. Reininghaus,[38] A. Reuzki,[41] J. Ridky,[31] F. Riehn,[77] M. Risse,[43] V. Rizi,[56,45] W. Rodrigues de Carvalho,[78] E. Rodriguez,[7,40] J. Rodriguez Rojo,[11] M. J. Roncoroni,[7] S. Rossoni,[42] M. Roth,[40] E. Roulet,[1] A. C. Rovero,[4] A. Saftoiu,[72] M. Saharan,[78] F. Salamida,[56,45] H. Salazar,[63] G. Salina,[50] J. D. Sanabria Gomez,[29] F. Sánchez,[7] E. M. Santos,[21] E. Santos,[31] F. Sarazin,[83] R. Sarmento,[71] R. Sato,[11] P. Savina,[89] C. M. Schäfer,[38] V. Scherini,[55,47] H. Schieler,[40] M. Schimassek,[33] M. Schimp,[37] D. Schmidt,[40] O. Scholten,[15,‡‡] H. Schoorlemmer,[78,79] P. Schovánek,[31] F. G. Schröder,[88,40] J. Schulte,[41] T. Schulz,[40] S. J. Sciutto,[3] M. Scornavacche,[7,40] A. Sedoski,[7] A. Segreto,[52,46] S. Sehgal,[37] S. U. Shivashankara,[74] G. Sigl,[42] K. Simkova,[15,14] F. Simon,[39] R. Smau,[72] R. Šmída,[87] P. Sommers,[§§] R. Squartini,[10] M. Stadelmaier,[48,58,40] S. Stanič,[74] J. Stasielak,[69] P. Stassi,[35] S. Strähnz,[38] M. Straub,[41] T. Suomijärvi,[36] A. D. Supanitsky,[7] Z. Svozilikova,[31] Z. Szadkowski,[70] F. Tairli,[13] A. Tapia,[28] C. Taricco,[62,51] C. Timmermans,[79,78] O. Tkachenko,[31] P. Tobiska,[31] C. J. Todero Peixoto,[19] B. Tomé,[71] Z. Torrès,[35] A. Travaini,[10] P. Travnicek,[31] M. Tueros,[3] M. Unger,[40] R. Uzeiroska,[37] L. Vaclavek,[32] M. Vacula,[32] J. F. Valdés Galicia,[67] L. Valore,[59,49] E. Varela,[63] V. Vašíčková,[37] A. Vásquez-Ramírez,[29] D. Veberič,[40] I. D. Vergara Quispe,[3] V. Verzi,[50] J. Vicha,[31] J. Vink,[81] S. Vorobiov,[74] C. Watanabe,[27] A. A. Watson,[‖‖] A. Weindl,[40]

L. Wiencke,[83] H. Wilczyński,[69] D. Wittkowski,[37] B. Wundheiler,[7] B. Yue,[37] A. Yushkov,[31] O. Zapparrata,[14] E. Zas,[77] D. Zavrtanik,[74,75] and M. Zavrtanik[75,74]

(Pierre Auger Collaboration)

[1]*Centro Atómico Bariloche and Instituto Balseiro (CNEA-UNCuyo-CONICET), San Carlos de Bariloche, Argentina*
[2]*Departamento de Física and Departamento de Ciencias de la Atmósfera y los Océanos, FCEyN, Universidad de Buenos Aires and CONICET, Buenos Aires, Argentina*
[3]*IFLP, Universidad Nacional de La Plata and CONICET, La Plata, Argentina*
[4]*Instituto de Astronomía y Física del Espacio (IAFE, CONICET-UBA), Buenos Aires, Argentina*
[5]*Instituto de Física de Rosario (IFIR)—CONICET/U.N.R. and Facultad de Ciencias Bioquímicas y Farmacéuticas U.N.R., Rosario, Argentina*
[6]*Instituto de Tecnologías en Detección y Astropartículas (CNEA, CONICET, UNSAM), and Universidad Tecnológica Nacional—Facultad Regional Mendoza (CONICET/CNEA), Mendoza, Argentina*
[7]*Instituto de Tecnologías en Detección y Astropartículas (CNEA, CONICET, UNSAM), Buenos Aires, Argentina*
[8]*International Center of Advanced Studies and Instituto de Ciencias Físicas, ECyT-UNSAM and CONICET, Campus Miguelete—San Martín, Buenos Aires, Argentina*
[9]*Laboratorio Atmósfera—Departamento de Investigaciones en Láseres y sus Aplicaciones—UNIDEF (CITEDEF-CONICET), Villa Martelli, Argentina*
[10]*Observatorio Pierre Auger, Malargüe, Argentina*
[11]*Observatorio Pierre Auger and Comisión Nacional de Energía Atómica, Malargüe, Argentina*
[12]*Universidad Tecnológica Nacional—Facultad Regional Buenos Aires, Buenos Aires, Argentina*
[13]*University of Adelaide, Adelaide, South Australia, Australia*
[14]*Université Libre de Bruxelles (ULB), Brussels, Belgium*
[15]*Vrije Universiteit Brussels, Brussels, Belgium*
[16]*Centro Brasileiro de Pesquisas Fisicas, Rio de Janeiro, RJ, Brazil*
[17]*Centro Federal de Educação Tecnológica Celso Suckow da Fonseca, Petropolis, Brazil*
[18]*Instituto Federal de Educação, Ciência e Tecnologia do Rio de Janeiro (IFRJ), RJ, Brazil*
[19]*Universidade de São Paulo, Escola de Engenharia de Lorena, Lorena, SP, Brazil*
[20]*Universidade de São Paulo, Instituto de Física de São Carlos, São Carlos, SP, Brazil*
[21]*Universidade de São Paulo, Instituto de Física, São Paulo, SP, Brazil*
[22]*Universidade Estadual de Campinas (UNICAMP), IFGW, Campinas, SP, Brazil*
[23]*Universidade Estadual de Feira de Santana, Feira de Santana, Brazil*
[24]*Universidade Federal de Campina Grande, Centro de Ciencias e Tecnologia, Campina Grande, Brazil*
[25]*Universidade Federal do ABC, Santo André, SP, Brazil*
[26]*Universidade Federal do Paraná, Setor Palotina, Palotina, Brazil*
[27]*Universidade Federal do Rio de Janeiro, Instituto de Física, Rio de Janeiro, RJ, Brazil*
[28]*Universidad de Medellín, Medellín, Colombia*
[29]*Universidad Industrial de Santander, Bucaramanga, Colombia*
[30]*Charles University, Faculty of Mathematics and Physics, Institute of Particle and Nuclear Physics, Prague, Czech Republic*
[31]*Institute of Physics of the Czech Academy of Sciences, Prague, Czech Republic*
[32]*Palacky University, Olomouc, Czech Republic*
[33]*CNRS/IN2P3, IJCLab, Université Paris-Saclay, Orsay, France*
[34]*Laboratoire de Physique Nucléaire et de Hautes Energies (LPNHE), Sorbonne Université, Université de Paris, CNRS-IN2P3, Paris, France*
[35]*Université Grenoble Alpes, CNRS, Grenoble Institute of Engineering Univ. Grenoble Alpes, LPSC-IN2P3, 38000 Grenoble, France*
[36]*Université Paris-Saclay, CNRS/IN2P3, IJCLab, Orsay, France*
[37]*Bergische Universität Wuppertal, Department of Physics, Wuppertal, Germany*
[38]*Karlsruhe Institute of Technology (KIT), Institute for Experimental Particle Physics, Karlsruhe, Germany*
[39]*Karlsruhe Institute of Technology (KIT), Institut für Prozessdatenverarbeitung und Elektronik, Karlsruhe, Germany*
[40]*Karlsruhe Institute of Technology (KIT), Institute for Astroparticle Physics, Karlsruhe, Germany*
[41]*RWTH Aachen University, III. Physikalisches Institut A, Aachen, Germany*
[42]*Universität Hamburg, II. Institut für Theoretische Physik, Hamburg, Germany*
[43]*Universität Siegen, Department Physik—Experimentelle Teilchenphysik, Siegen, Germany*
[44]*Gran Sasso Science Institute, L'Aquila, Italy*
[45]*INFN Laboratori Nazionali del Gran Sasso, Assergi (L'Aquila), Italy*
[46]*INFN, Sezione di Catania, Catania, Italy*
[47]*INFN, Sezione di Lecce, Lecce, Italy*
[48]*INFN, Sezione di Milano, Milano, Italy*
[49]*INFN, Sezione di Napoli, Napoli, Italy*

[50]INFN, Sezione di Roma "Tor Vergata", Roma, Italy
[51]INFN, Sezione di Torino, Torino, Italy
[52]Istituto di Astrofisica Spaziale e Fisica Cosmica di Palermo (INAF), Palermo, Italy
[53]Osservatorio Astrofisico di Torino (INAF), Torino, Italy
[54]Politecnico di Milano, Dipartimento di Scienze e Tecnologie Aerospaziali, Milano, Italy
[55]Università del Salento, Dipartimento di Matematica e Fisica "E. De Giorgi", Lecce, Italy
[56]Università dell'Aquila, Dipartimento di Scienze Fisiche e Chimiche, L'Aquila, Italy
[57]Università di Catania, Dipartimento di Fisica e Astronomia "Ettore Majorana", Catania, Italy
[58]Università di Milano, Dipartimento di Fisica, Milano, Italy
[59]Università di Napoli "Federico II", Dipartimento di Fisica "Ettore Pancini", Napoli, Italy
[60]Università di Palermo, Dipartimento di Fisica e Chimica "E. Segrè", Palermo, Italy
[61]Università di Roma "Tor Vergata", Dipartimento di Fisica, Roma, Italy
[62]Università Torino, Dipartimento di Fisica, Torino, Italy
[63]Benemérita Universidad Autónoma de Puebla, Puebla, México
[64]Unidad Profesional Interdisciplinaria en Ingeniería y Tecnologías Avanzadas del Instituto Politécnico Nacional (UPIITA-IPN), México, D.F., México
[65]Universidad Autónoma de Chiapas, Tuxtla Gutiérrez, Chiapas, México
[66]Universidad Michoacana de San Nicolás de Hidalgo, Morelia, Michoacán, México
[67]Universidad Nacional Autónoma de México, México, D.F., México
[68]Universidad Nacional de San Agustin de Arequipa, Facultad de Ciencias Naturales y Formales, Arequipa, Peru
[69]Institute of Nuclear Physics PAN, Krakow, Poland
[70]University of Łódź, Faculty of High-Energy Astrophysics, Łódź, Poland
[71]Laboratório de Instrumentação e Física Experimental de Partículas—LIP and Instituto Superior Técnico—IST, Universidade de Lisboa—UL, Lisboa, Portugal
[72]"Horia Hulubei" National Institute for Physics and Nuclear Engineering, Bucharest-Magurele, Romania
[73]Institute of Space Science, Bucharest-Magurele, Romania
[74]Center for Astrophysics and Cosmology (CAC), University of Nova Gorica, Nova Gorica, Slovenia
[75]Experimental Particle Physics Department, J. Stefan Institute, Ljubljana, Slovenia
[76]Universidad de Granada and C.A.F.P.E., Granada, Spain
[77]Instituto Galego de Física de Altas Enerxías (IGFAE), Universidade de Santiago de Compostela, Santiago de Compostela, Spain
[78]IMAPP, Radboud University Nijmegen, Nijmegen, The Netherlands
[79]Nationaal Instituut voor Kernfysica en Hoge Energie Fysica (NIKHEF), Science Park, Amsterdam, The Netherlands
[80]Stichting Astronomisch Onderzoek in Nederland (ASTRON), Dwingeloo, The Netherlands
[81]Universiteit van Amsterdam, Faculty of Science, Amsterdam, The Netherlands
[82]Case Western Reserve University, Cleveland, Ohio, USA
[83]Colorado School of Mines, Golden, Colorado, USA
[84]Department of Physics and Astronomy, Lehman College, City University of New York, Bronx, New York, USA
[85]Michigan Technological University, Houghton, Michigan, USA
[86]New York University, New York, New York, USA
[87]University of Chicago, Enrico Fermi Institute, Chicago, Illinois, USA
[88]University of Delaware, Department of Physics and Astronomy, Bartol Research Institute, Newark, Delaware, USA
[89]University of Wisconsin-Madison, Department of Physics and WIPAC, Madison, Wisconsin, USA

(Received 10 June 2024; revised 23 October 2024; accepted 30 October 2024; published 13 January 2025)

[*]Max-Planck-Institut für Radioastronomie, Bonn, Germany.
[†]Institut universitaire de France (IUF), IUF, France.
[‡]Colorado State University, Fort Collins, Colorado, USA.
[§]Present address: Agenzia Spaziale Italiana (ASI), Via del Politecnico 00133, Roma, Italy.
[‖]Present address: Graduate School of Science, Osaka Metropolitan University, Osaka, Japan.
[¶]Present address: ECAP, Erlangen, Germany.
[**]Fermi National Accelerator Laboratory, Fermilab, Batavia, Illinois, USA.
[††]Louisiana State University, Baton Rouge, Louisiana, USA.
[‡‡]Also at Kapteyn Institute, University of Groningen, Groningen, The Netherlands.
[§§]Pennsylvania State University, University Park, Pennsylvania, USA.
[‖‖]School of Physics and Astronomy, University of Leeds, Leeds, United Kingdom.

We present measurements of the atmospheric depth of the shower maximum X_{max}, inferred for the first time on an event-by-event level using the surface detector of the Pierre Auger Observatory. Using deep learning, we were able to extend measurements of the X_{max} distributions up to energies of 100 EeV (10^{20} eV), not yet revealed by current measurements, providing new insights into the mass composition of cosmic rays at extreme energies. Gaining a 10-fold increase in statistics compared to the fluorescence detector data, we find evidence that the rate of change of the average X_{max} with the logarithm of energy features three breaks at $6.5 \pm 0.6(\mathrm{stat}) \pm 1(\mathrm{syst})$ EeV, $11 \pm 2(\mathrm{stat}) \pm 1(\mathrm{syst})$ EeV, and $31 \pm 5(\mathrm{stat}) \pm 3(\mathrm{syst})$ EeV, in the vicinity to the three prominent features (ankle, instep, suppression) of the cosmic-ray flux. The energy evolution of the mean and standard deviation of the measured X_{max} distributions indicates that the mass composition becomes increasingly heavier and purer, thus being incompatible with a large fraction of light nuclei between 50 and 100 EeV.

DOI: 10.1103/PhysRevLett.134.021001

Introduction—The arrival directions, energy spectrum, and mass composition are the three important pillars of cosmic ray research. A sound interpretation of the three measurements and their energy dependence, both individually and jointly, is pivotal for a deep understanding of the nature of cosmic rays, including their origin and propagation, and enables the study of astrophysical models. With energies larger than 1 EeV (10^{18} eV), ultra-high-energy cosmic rays (UHECRs) are the most energetic particles ever measured by humankind. One of the lasting puzzles is the origin of the suppression of the cosmic-ray flux observed at around 50 EeV [1–4]. A precise measurement of the UHECR mass composition can deliver insights into whether the suppression is caused by the interaction of the particles with the cosmic background photons [5,6], a sign of the maximum energy reached in cosmic accelerators [7], or a combination of both [8,9]. Because of the low flux at ultrahigh energies, the primary composition cannot be measured directly but can only be studied by indirectly analyzing the properties of the induced air showers. Information on the primary mass can be obtained by measuring the atmospheric depth of the shower maximum X_{max}, the depth at which the number of secondary particles reaches its maximum. Investigating the measured X_{max} distribution, as a function of energy, in terms of its mean and standard deviation (fluctuations), $\langle X_{\mathrm{max}} \rangle$ and $\sigma(X_{\mathrm{max}})$, enables us to study the UHECR mass composition [10–12]. Heavier particles feature, on average, a smaller X_{max} since more subshowers are created sharing the primary energy. This results in a maximum higher in the atmosphere and motivates the investigation of the first moment $\langle X_{\mathrm{max}} \rangle$ of the distribution. Further, the shower-to-shower fluctuations, i.e., the second moment $\sigma(X_{\mathrm{max}})$ of the distribution, is also mass-sensitive. Because of the smaller cross section and the development of fewer subshowers, cascades induced by lighter primary particles are subject to larger fluctuations. The fluctuations $\sigma(X_{\mathrm{max}})$ are sensitive to both the primary mass and the degree of mixing of the primary beam [13], compared to $\langle X_{\mathrm{max}} \rangle$, almost insensitive to the uncertainties in the hadronic interaction models.

Using fluorescence telescopes, X_{max} can be directly reconstructed by observing the longitudinal shower development. Nevertheless, due to the observations being confined to dark and moonless nights, the duty cycle is limited. In contrast, sparse surface-detector arrays have a duty cycle close to 100% and sample the secondary shower particles at the ground. Thus, they cannot directly observe X_{max}, making its reconstruction challenging. However, information about the shower development and X_{max} is contained in the lateral number density and distribution of arrival times of particles reaching the ground. By studying the risetimes of the time-dependent signals, conclusions on the average composition have already been drawn in the past [14]. However, to infer the UHECR mass composition beyond mere $\langle X_{\mathrm{max}} \rangle$ measurements, more sophisticated methods are needed to fully exploit the complex data. The advent of deep learning [15,16] provides new analysis techniques for large and complex datasets. First approaches have already been successfully applied to LHC data [17] and physics in general [18]. The recent progress offers supplementary and improved reconstruction algorithms for neutrino [19–21] and cosmic-ray observatories [22]. This includes the deep-learning-based reconstruction of X_{max} [23–26] and muon signals [27] using the temporal structure of signals measured by the Surface Detector of the Pierre Auger Observatory.

In this work, the novel reconstruction technique is used for the first time to study the mass composition of UHECRs in terms of $\langle X_{\mathrm{max}} \rangle$ and $\sigma(X_{\mathrm{max}})$ in the energy range from 3 to 100 EeV. With about 50000 events, this is the most comprehensive study of the UHECR mass composition and the first measurement of $\sigma(X_{\mathrm{max}})$ beyond 50 EeV. A comprehensive discussion of the analysis, including the technical details of the analysis, is given in an accompanying publication [28].

Methodology—In the past two decades, our understanding of UHECRs has grown enormously due to the construction of the Pierre Auger Observatory [29] and the Telescope Array Project [30]. The Pierre Auger Observatory is the world's largest UHECR experiment

and a hybrid instrument combining surface detectors and fluorescence telescopes to measure cosmic-ray-induced air showers. In total, 1660 water-Cherenkov detectors, spanning 3000 km^2, are arranged in a triangular 1500-meter-grid and form the surface detector (SD)—the centerpiece of the Observatory with a duty cycle close to 100%. The SD is overlooked by 24 telescopes located at four sites that form the fluorescence detector (FD). Additionally, three high-elevation telescopes overlook an infilled array of 61 stations with 750 m spacing that enable measurements below 3 EeV. The requirement for dark and moonless nights limits the duty cycle of the FD to about 15%.

The typical size of an air-shower footprint with $E > 10$ EeV amounts to tens of km^2, and it usually triggers more than ten stations of the SD. Each station is equipped with three photomultiplier tubes (PMTs) that record the time-dependent responses to shower particles digitized and sampled in steps of 25 ns. The resulting three traces are then calibrated in units of VEM (vertical equivalent muons), i.e., the average signal produced by muons traversing the detector vertically, provided by an *in situ* calibration on a minute timescale using atmospheric muons. Several station-level measurements characterize each event in our analysis: the arrival time of the first particles at the respective station and, for each PMT, a trace of 3 μs time length (120 time steps) containing the signal.

In this work, we use two different datasets: a hybrid dataset, featuring both an FD and SD reconstruction used to calibrate the reconstruction algorithm to the X_{max} scale of the FD, and the full SD dataset for performing the high-statistics measurement of $\langle X_{\mathrm{max}} \rangle$ and $\sigma(X_{\mathrm{max}})$. We only select events with an energy $E_{\mathrm{SD}} > 3$ EeV to ensure full trigger efficiency [31], require a zenith angle $\theta < 60°$, and a hexagon of working stations around the station with the largest signal [32]. Furthermore, a fiducial SD cut is applied [28] to ensure an unbiased X_{max} measurement, accepting only events inside a zenith-angle range where the absolute X_{max} reconstruction bias of the DNN is smaller than 10 $\mathrm{g\,cm^{-2}}$. After selection, the SD dataset comprises 48824 events collected between 1 January 2004 and 31 August 2018. For the calibration of the novel algorithm, hybrid events featuring both an FD and SD reconstruction are used. We accept only FD events with good atmospheric conditions and small uncertainties on the observed shower profile. In particular, we reject events with X_{max} reconstructed outside the telescope field of view. To avoid a selection bias, as X_{max} depends on the primary mass, we apply a fiducial cut that ensures uniform acceptance for most of the X_{max} distribution [12]. 1642 hybrid events remain after selection.

Information on the primary particle mass is encoded in the temporal structure of the recorded SD signals, i.e., the signal traces and arrival times [14,33]. The X_{max} reconstruction applied in this work is based on a deep neural network (DNN) to exploit the patterns of different shower components in the time-resolved particle density. For example, muons usually produce signal spikes, while the signals from each electron, positron, and photon are individually smaller and are spread out in time because of multiple scattering [34]. In the first part, the shape of signal traces is analyzed using long-short term memory (LSTM) layers [35], and in the second part, the spatial distribution of the signal footprint induced on the SD grid is exploited using convolutional layers [36]. The DNN was trained using the simulated detector responses [37] of 400 000 showers induced by proton, helium, oxygen, and iron with energies from 1 to 160 EeV. The showers were simulated with CORSIKA [38] using the EPOS-LHC interaction model. For more details on the algorithm, we refer to Ref. [23].

After correcting [28] the reconstruction for aging effects [39,40] and temporal variations, we use hybrid data to calibrate the SD-based DNN algorithm to the FD X_{max} scale. Since UHECRs feature energies above what can be reached with human-built accelerators, air-shower simulations make use of extrapolated collider data and phenomenological modeling that differ for each hadronic interaction model. As fluorescence telescopes directly observe X_{max}, they offer the possibility of removing the dependence of the SD-based algorithm on the particular interaction model and significantly reduce the systematic uncertainties of the $\langle X_{\mathrm{max}} \rangle$ measurement. By studying the difference between the DNN predictions and the FD observations, we observe an offset of (-31.7 ± 0.7) $\mathrm{g\,cm^{-2}}$ compatible within uncertainties to be independent of energy ($\Delta X_{\mathrm{max}} < 6$ $\mathrm{g\,cm^{-2}\,decade^{-1}}$), as determined by a fit. The observed offset is larger than the expected differences by up to -15 $\mathrm{g\,cm^{-2}}$ from studies using various hadronic interaction models [23,28]. This indicates that the current generation of hadronic interaction models may not describe the measured data entirely, which is consistent with previous analyses that suggest inadequacies in the description of muon profiles [14,33,41,42], as well as the longitudinal profiles in general [43].

In Fig. 1, the correlation between the X_{max} reconstruction of the DNN and the FD is shown after calibration and is a significant improvement compared to previous analyses [14]. The found correlation and resolution of the DNN are in excellent agreement with simulation studies [23] verifying the reconstruction and indicating that the fluctuations are well modeled. This can be expected, as the shower fluctuations are significantly driven by the fluctuations of the first interaction [44], which is relatively similar across hadronic interaction models, and additionally, the relative fluctuations of the number of muons seem to be properly modeled [42].

Results and discussion—To investigate the evolution of the UHECR mass composition, we study the first and second moments of the X_{max} distributions in Fig. 2 measured by the SD as a function of energy E. We use

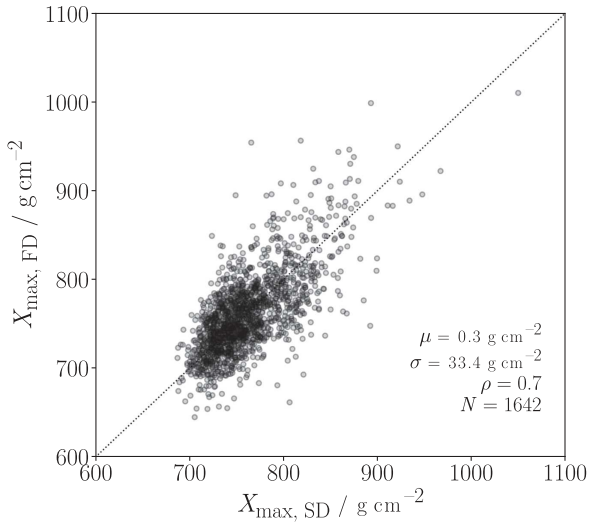

FIG. 1. Application of the DNN to hybrid data. Correlation between fluorescence observations of the FD and DNN predictions using SD data after calibration. The 1642 events show a clear correlation of $\rho = 0.7$ and a bias $\mu < 1$ g cm^{-2}.

bins of $\Delta\log_{10}(E/\mathrm{eV}) = 0.1$ and an integral bin beyond $10^{19.9}$ eV. The gray open squares denote FD measurements [45] of the same data-taking period, and black circles the SD-based DNN measurement of this work, extending the X_{max} measurements to the highest energies. Whereas vertical bars indicate statistical uncertainties obtained via bootstrapping, brackets denote systematic uncertainties. The red (blue) lines mark predictions [46] from three hadronic interaction models [47–49] for a pure proton (iron) composition. The systematic uncertainties of $\langle X_{\mathrm{max}}\rangle$ range from 9 to 13 g cm^{-2} and are dominated by the hybrid calibration and the uncertainty of the FD X_{max} scale. The systematic uncertainties of the $\sigma(X_{\mathrm{max}})$ measurement are dominated by the composition bias of the energy measurement and the interaction-model bias of the DNN and are in the order of ± 6 g cm^{-2}. This bias was conservatively estimated using a simulation study with various realistic composition scenarios, the measured UHECR energy spectrum [4], and by considering systematic uncertainties on the reconstruction [28].

The $\langle X_{\mathrm{max}}\rangle$ measured with the SD shows excellent agreement with FD observations as shown in Fig. 2(a). The measurement shows a transition from a relatively light to a heavier composition, confirming the observation of previous analyses [10,11,14,45,50] and extending our measurements to 100 EeV. As shown in Fig. 2(b), with rising energy, the fluctuations diminish and agree well with previous FD measurements. The observation of decreasing $\sigma(X_{\mathrm{max}})$ implies that besides becoming heavier, the mass composition also has to be rather pure. This yields a consistent interpretation [28] of the primary UHECR composition when combined with measurements of $\langle X_{\mathrm{max}}\rangle$. The small fluctuations disfavor a substantial fraction of light particles at the highest energies and, at the same time, indicate that the observed suppression in the energy spectrum cannot be entirely ascribed to effects of extragalactic propagation [8,9].

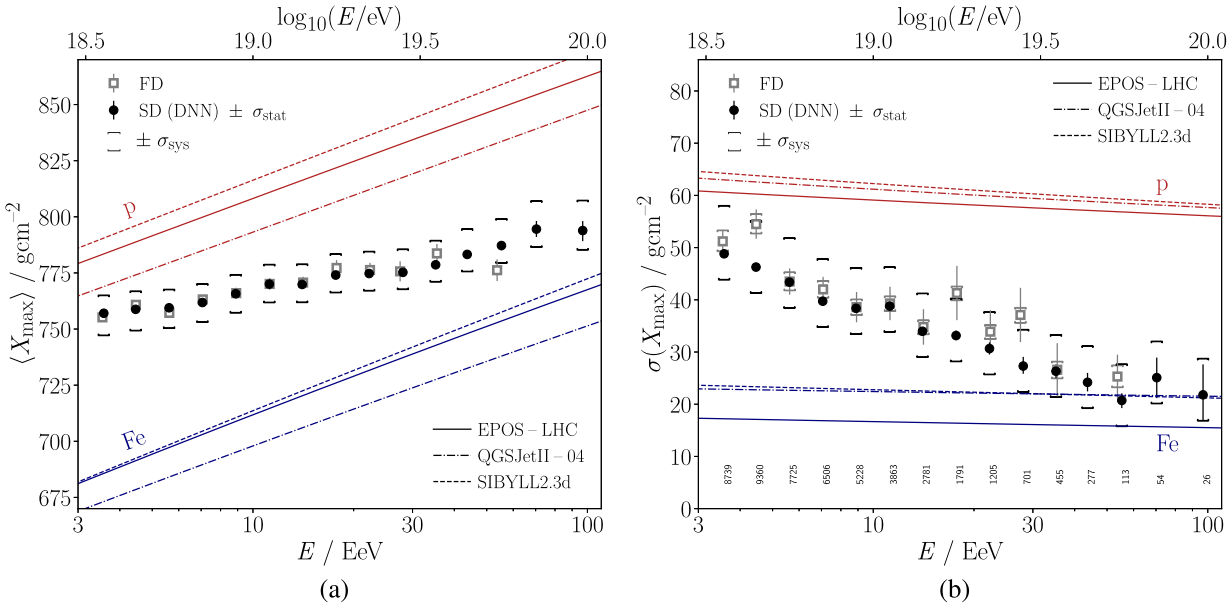

FIG. 2. Energy evolution of (a) the mean depth of shower maximum $\langle X_{\mathrm{max}}\rangle$ and (b) the fluctuations of shower maximum $\sigma(X_{\mathrm{max}})$ as determined using the FD reconstruction (gray open squares) [45] and the SD-based DNN predictions (black circles). Red (blue) lines indicate expectations for a pure proton (iron) composition for various hadronic models. The number of events in each bin is indicated in panel (b).

A change in the composition of the primary mass can be studied by investigating the *elongation rate*:

$$D_{10} \hat{=} \frac{\mathrm{d}\langle X_{\mathrm{max}}\rangle}{\mathrm{d}\log_{10}E} = \hat{D}_{10}\left(1 - \frac{\mathrm{d}\langle \ln A\rangle}{\mathrm{d}\ln E}\right),$$

defined by the change of $\langle X_{\mathrm{max}}\rangle$ in one decade of energy and comparing it to an expected elongation rate $\hat{D}_{10}$ obtained using simulations, which is rather universal across primary masses A and interaction models and ranges from 55 to 60 $\mathrm{g\,cm^{-2}\,decade^{-1}}$. A linear fit with a constant elongation rate yields $D_{10} = 24.1 \pm 1.2\ \mathrm{g\,cm^{-2}\,decade^{-1}}$, in good agreement with the FD measurements in this energy range $\left((26 \pm 2)\ \mathrm{g\,cm^{-2}\,decade^{-1}}\right)$, but does not describe well our data with $\chi^2/\mathrm{d.o.f.} = 46.7/13$. Because of the significant increase in statistics, we find evidence for a distinctive structure in the elongation rate when studying the evolution of $\langle X_{\mathrm{max}}\rangle$ using functions piecewise linear in $\log(E/\mathrm{eV})$. The observed elongation rate model, shown as a red line in the top panel of Fig. 3, features three breaks ($\chi^2/\mathrm{dof} = 10.4/7$). Using Wilks's theorem, we compared this model with the null hypothesis of a constant elongation rate and found that we can reject the constant elongation rate model at a statistical significance of 4.6σ. Considering energy-dependent systematic uncertainties, the significance level for rejecting a constant elongation rate reduces to 4.4σ. We furthermore studied the compatibility of the FD data with our new elongation rate model and observed a good agreement ($\chi^2/\mathrm{d.o.f.} = 12.8/12$).

The null hypothesis of a model describing the SD with only two breaks at lower energies (E_1, E_2), positioned close to the ankle and instep, can be rejected at a statistical significance level of 3.3σ using the found elongation rate model and shows a stronger dependence on systematic uncertainties. A single-break model can be rejected with a significance of 4.4σ and consistently remains above the 3σ level when including systematics. The fitted parameters of the model with three breaks are summarized in Table I together with the positions of the energy of spectrum features measured using the SD and the infill array with 750 m spacing. As shown as a continuous red line in the top panel of Fig. 3, the found breaks in the evolution of $\langle X_{\mathrm{max}}\rangle$ are observed close to the ankle, instep, and suppression features of the energy spectrum [51], shown in the bottom panel of Fig. 3. The hatched gray regions denote statistical and systematic uncertainties of the position of the features. Note that distinct features do not have to emerge at similar energies for an astrophysical interpretation of the energy spectrum and its composition. For example, the break in the elongation rate observed using the FD of the Observatory around 2 EeV [11], shown as a dotted gray line in the top panel of Fig. 3, is physically interpreted [8,9,52] in association with the ankle, which has been discovered at 5 EeV.

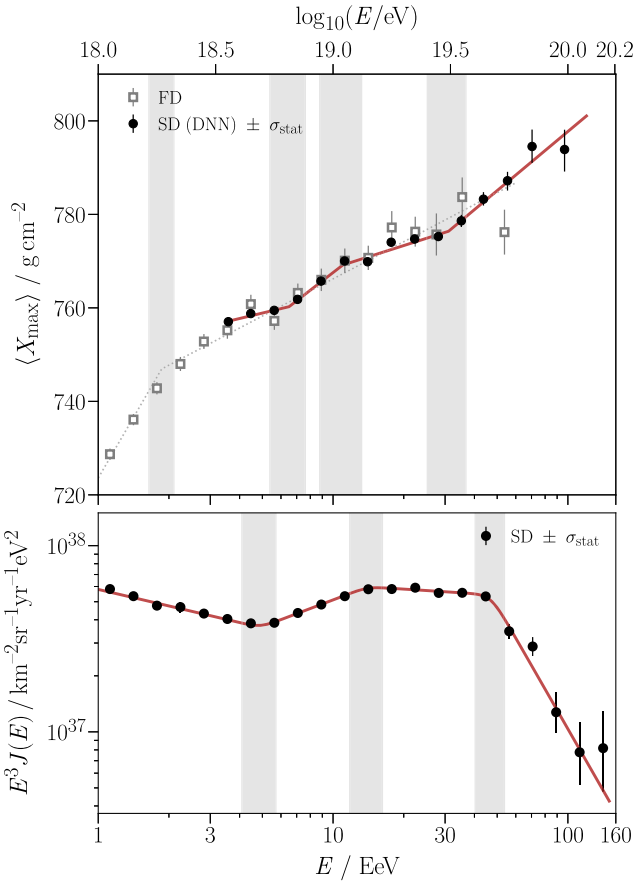

FIG. 3. Positions of breaks in the elongation rate compared to energy spectrum features. Top: Evolution of $\langle X_{\mathrm{max}}\rangle$ as a function of energy for the SD (black) and the FD (gray) [45]. The red line indicates the elongation model found using the SD, and the dotted gray line using the FD. Bottom: Combined energy spectrum [51] as measured using the SD 1500 m array and the low energy 750 m infill array of the Observatory. Gray regions indicate the uncertainties in the energy of the found breaks and features.

TABLE I. Best-fit parameters with statistical and systematic uncertainties for the identified model that features three changes in the elongation rate (D_0, D_1, D_2, D_3) at energies (E_1, E_2, E_3) and an offset b of $\langle X_{\mathrm{max}}\rangle$ at 1 EeV. The positions of the features of the energy spectrum [51] are also given.

Parameter val $\pm\ \sigma_{\mathrm{stat}} \pm \sigma_{\mathrm{syst}}$	3-Break model val $\pm\ \sigma_{\mathrm{stat}} \pm \sigma_{\mathrm{syst}}$	Energy spectrum val $\pm\ \sigma_{\mathrm{stat}} \pm \sigma_{\mathrm{syst}}$
$b/\mathrm{g\,cm^{-2}}$	$750.5 \pm 3 \pm 13$	
$D_0/\mathrm{g\,cm^{-2}\,decade^{-1}}$	$12 \pm 5 \pm 6$	
E_1/EeV	$6.5 \pm 0.6 \pm 1$	$4.9 \pm 0.1 \pm 0.8$
$D_1/\mathrm{g\,cm^{-2}\,decade^{-1}}$	$39 \pm 5 \pm 14$	
E_2/EeV	$11 \pm 2 \pm 1$	$14 \pm 1 \pm 2$
$D_2/\mathrm{g\,cm^{-2}\,decade^{-1}}$	$16 \pm 3 \pm 6$	
E_3/EeV	$31 \pm 5 \pm 3$	$47 \pm 3 \pm 6$
$D_3/\mathrm{g\,cm^{-2}\,decade^{-1}}$	$42 \pm 9 \pm 12$	

Interestingly, the composition model discussed in Ref. [9] (Figs. 3 and 6), derived by taking into account astrophysical scenarios, including extragalactic propagation and fitting the energy spectrum measured by the SD and the X_{max} distribution observed by the FD, predicts three breaks at positions matching our results. An investigation of this finding to obtain a detailed understanding of the astrophysical origin of these breaks is ongoing.

We also studied the evolution of $\sigma(X_{\mathrm{max}})$ [see Fig. 2(b)] to identify a potentially similar underlying structure. We observe a decrease in fluctuations, while the elongation rate implies a change towards a heavier composition. Consistently, we find no substantial change in the fluctuations $\sigma(X_{\mathrm{max}})$ at the regions—between the ankle and the instep, and above the suppression—where the elongation rate of $\langle X_{\mathrm{max}}\rangle$ is closer to that of a constant composition. While being compatible with the data ($\chi/\mathrm{ndf} = 10.3/10$), a model featuring three breaks at positions fixed to those found in the elongation rate is statistically not significant (2.2σ) if compared to a linear decrease in $\sigma(X_{\mathrm{max}})$. Note that changes in the primary mass composition are not reflected in the same way in the energy evolution of $\langle X_{\mathrm{max}}\rangle$ and $\sigma(X_{\mathrm{max}})$ [13]. A simple transition between two primary species at a constant rate corresponds to a linear dependence of $\langle X_{\mathrm{max}}\rangle$ on $\log(E)$ but to a nonlinear behavior of $\sigma(X_{\mathrm{max}})$, for which, thus, the application of a broken-line model is inappropriate. For a larger number of primary species with unknown proportions, a specific model for the interpretation of $\sigma(X_{\mathrm{max}})$ cannot be defined. More sophisticated studies on the astrophysical origin of the features in the mass composition and the energy spectrum are ongoing and will, jointly with the upgrade of the observatory AugerPrime [53], offer new insights into the nature of UHECRs.

Summary—We have performed a measurement of $\langle X_{\mathrm{max}}\rangle$ and $\sigma(X_{\mathrm{max}})$ for cosmic rays with energies between 3 and 100 EeV to investigate their mass composition. The method relies on the time-dependent signals recorded by the SD of the Pierre Auger Observatory. After training our deep learning model on simulated SD data, we used measured hybrid data to crosscheck and cross-calibrate our algorithm using the FD of the Observatory to remove mismatches between simulations and measured data. With the calibrated DNN, we obtained a 10-fold increase in the size of the X_{max} dataset for $E > 5$ EeV compared to the FD measurements and found a consistent picture of the $\langle X_{\mathrm{max}}\rangle$ and $\sigma(X_{\mathrm{max}})$ measurements. At lower energies, our measurements are in excellent agreement with fluorescence observations, indicating a light and mixed mass composition. At the highest, so far inaccessible energies, we report a purer and heavier composition, confirming the trend suggested by the FD data. The observation of small fluctuations in X_{max} beyond 50 EeV excludes a significant fraction of light nuclei at the highest energies and further excludes the flux suppression to be generated by protons interacting with the cosmic microwave background. However, this observation is insufficient to disentangle whether the suppression arises from the maximum injection energy at the sources, propagation effects, or a combination of both. Because of the substantial rise in statistics, we have found evidence at a level of 4.4σ for a characteristic structure in the evolution of the mass composition beyond a constant elongation rate. The model describing our data best features three breaks. Interestingly, the identified breaks in the elongation rate model are observed to be in proximity of the ankle, instep, and suppression features in the energy spectrum, where changes in the spectral index have been reported [4]. More statistics are needed to study the nature of the identified breaks and, particularly, investigate the existence of the third break. We have demonstrated the large potential of applying deep neural networks to astroparticle physics, particularly in the analysis of low-level data. Our approach comprises detailed systematic uncertainties, including the cross-calibration with a complementary detector, highlighting the importance of an independent data set for calibration and validation of these powerful algorithms.

The Pierre Auger Observatory is now being upgraded, which includes the deployment of scintillators and radio antennas on top of each SD station. The new detectors, combined with the emerging capabilities of machine-learning-based algorithms, offer unique prospects for accurate composition studies [54,55] and increase our understanding of cosmic rays at ultrahigh energies.

Acknowledgments—The successful installation, commissioning, and operation of the Pierre Auger Observatory would not have been possible without the strong commitment and effort from the technical and administrative staff in Malargüe. We are very grateful to the following agencies and organizations for financial support: Argentina—Comisión Nacional de Energía Atómica; Agencia Nacional de Promoción Científica y Tecnológica (ANPCyT); Consejo Nacional de Investigaciones Científicas y Técnicas (CONICET); Gobierno de la Provincia de Mendoza; Municipalidad de Malargüe; NDM Holdings and Valle Las Leñas; in gratitude for their continuing cooperation over land access; Australia—the Australian Research Council; Belgium—Fonds de la Recherche Scientifique (FNRS); Research Foundation Flanders (FWO), Marie Curie Action of the European Union Grant No. 101107047; Brazil—Conselho Nacional de Desenvolvimento Científico e Tecnológico (CNPq); Financiadora de Estudos e Projetos (FINEP); Fundação de Amparo à Pesquisa do Estado de Rio de Janeiro (FAPERJ); São Paulo Research Foundation (FAPESP) Grants No. 2019/10151-2, No. 2010/07359-6 and No. 1999/05404-3; Ministério da Ciência, Tecnologia, Inovações e Comunicações (MCTIC); Czech Republic—GACR 24-13049S, CAS LQ100102401, MEYS

LM2023032, CZ.02.1.01/0.0/0.0/16_013/0001402, CZ.02.1.01/0.0/0.0/18_046/0016010 and CZ.02.1.01/0.0/0.0/17_049/0008422 and CZ.02.01.01/00/22_008/0004632; France—Centre de Calcul IN2P3/CNRS; Centre National de la Recherche Scientifique (CNRS); Conseil Régional Ile-de-France; Département Physique Nucléaire et Corpusculaire (PNC-IN2P3/CNRS); Département Sciences de l'Univers (SDU-INSU/CNRS); Institut Lagrange de Paris (ILP) Grant No. LABEX ANR-10-LABX-63 within the Investissements d'Avenir Programme Grant No. ANR-11-IDEX-0004-02; Germany—Bundesministerium für Bildung und Forschung (BMBF); Deutsche Forschungsgemeinschaft (DFG); Finanzministerium Baden-Württemberg; Helmholtz Alliance for Astroparticle Physics (HAP); Helmholtz-Gemeinschaft Deutscher Forschungszentren (HGF); Ministerium für Kultur und Wissenschaft des Landes Nordrhein-Westfalen; Ministerium für Wissenschaft, Forschung und Kunst des Landes Baden-Württemberg; Italy—Istituto Nazionale di Fisica Nucleare (INFN); Istituto Nazionale di Astrofisica (INAF); Ministero dell'Università e della Ricerca (MUR); CETEMPS Center of Excellence; Ministero degli Affari Esteri (MAE), ICSC Centro Nazionale di Ricerca in High Performance Computing, Big Data and Quantum Computing, funded by European Union NextGenerationEU, reference code CN_00000013; México—Consejo Nacional de Ciencia y Tecnología (CONACYT) No. 167733; Universidad Nacional Autónoma de México (UNAM); PAPIIT DGAPA-UNAM; The Netherlands—Ministry of Education, Culture and Science; Netherlands Organisation for Scientific Research (NWO); Dutch national e-infrastructure with the support of SURF Cooperative; Poland—Ministry of Education and Science, Grants No. DIR/WK/2018/11 and No. 2022/WK/12; National Science Centre, Grants No. 2016/22/M/ST9/00198, No. 2016/23/B/ST9/01635, No. 2020/39/B/ST9/01398, and No. 2022/45/B/ST9/02163; Portugal—Portuguese national funds and FEDER funds within Programa Operacional Factores de Competitividade through Fundação para a Ciência e a Tecnologia (COMPETE); Romania—Ministry of Research, Innovation and Digitization, CNCS-UEFISCDI, Contract No. 30N/2023 under Romanian National Core Program LAPLAS VII, Grant No. PN 23 21 01 02 and Project No. PN-III-P1-1.1-TE-2021-0924/TE57/2022, within PNCDI III; Slovenia—Slovenian Research Agency, Grants P1-0031, P1-0385, I0-0033, N1-0111; Spain—Ministerio de Ciencia e Innovación/Agencia Estatal de Investigación (PID2019–105544 GB-I00, PID2022-140510NB-I00, and RYC2019-027017-I), Xunta de Galicia (CIGUS Network of Research Centers, Consolidación 2021 GRC GI-2033, ED431C-2021/22, and ED431F-2022/15), Junta de Andalucía (SOMM17/6104/UGR and P18-FR-4314), and the European Union (Marie Sklodowska-Curie 101065027 and ERDF); USA—Department of Energy, Contracts No. DE-AC02-07CH11359, No. DE-FR02-04ER41300, No. DE-FG02-99ER41107, and No. DE-SC0011689; National Science Foundation, Grant No. 0450696; The Grainger Foundation; Marie Curie-IRSES/EPLANET; European Particle Physics Latin American Network; and UNESCO.

[1] R. U. Abbasi *et al.* (High Resolution Fly's Eye Collaboration), Phys. Rev. Lett. **100**, 101101 (2008).
[2] J. Abraham *et al.* (Pierre Auger Collaboration), Phys. Rev. Lett. **101**, 061101 (2008).
[3] T. Abu-Zayyad *et al.* (Telescope Array Project Collaboration), Astrophys. J. Lett. **768**, L1 (2013).
[4] A. Aab *et al.* (Pierre Auger Collaboration), Phys. Rev. Lett. **125**, 121106 (2020).
[5] K. Greisen, Phys. Rev. Lett. **16**, 748 (1966).
[6] G. T. Zatsepin and V. A. Kuzmin, JETP Lett. **4**, 78 (1966).
[7] D. Allard, N. G. Busca, G. Decerprit, A. V. Olinto, and E. Parizot, J. Cosmol. Astropart. Phys. 10 (2008) 033.
[8] A. Aab *et al.* (Pierre Auger Collaboration), J. Cosmol. Astropart. Phys. 04 (2017) 038.
[9] A. Abdul Halim *et al.* (Pierre Auger Collaboration), J. Cosmol. Astropart. Phys. 05 (2023) 024.
[10] J. Abraham *et al.* (Pierre Auger Collaboration), Phys. Rev. Lett. **104**, 091101 (2010).
[11] A. Aab *et al.* (Pierre Auger Collaboration), Phys. Rev. D **90**, 122005 (2014).
[12] A. Aab *et al.* (Pierre Auger Collaboration), Phys. Rev. D **90**, 122006 (2014).
[13] P. Abreu *et al.* (Pierre Auger Collaboration), J. Cosmol. Astropart. Phys. 02 (2013) 026.
[14] A. Aab *et al.* (Pierre Auger Collaboration), Phys. Rev. D **96**, 122003 (2017).
[15] Y. LeCun, Y. Bengio, and G. Hinton, Nature (London) **521**, 436 (2015).
[16] I. Goodfellow, Y. Bengio, and A. Courville, *Deep Learning* (MIT Press, Cambridge, MA, 2016).
[17] D. Guest, K. Cranmer, and D. Whiteson, Annu. Rev. Nucl. Part. Sci. **68**, 161 (2018).
[18] M. Erdmann, J. Glombitza, G. Kasieczka, and U. Klemradt, *Deep Learning for Physics Research* (World Scientific, Singapore, 2021), 10.1142/12294.
[19] R. Abbasi *et al.* (IceCube Collaboration), J. Instrum. **16**, P07041 (2021).
[20] S. Aiello *et al.* (KM3NeT Collaboration), J. Instrum. **15**, P10005 (2020).
[21] R. Abbasi *et al.* (IceCube Collaboration), Science **380**, 1338 (2023).
[22] M. Erdmann, J. Glombitza, and D. Walz, Astropart. Phys. **97**, 46 (2018).
[23] A. Aab *et al.* (Pierre Auger Collaboration), J. Instrum. **16**, P07019 (2021).
[24] J. Glombitza on behalf of the Pierre Auger Collaboration, Proc. Sci. ICRC2019 (**2019**) 270.
[25] J. Glombitza on behalf of the Pierre Auger Collaboration, Proc. Sci. ICRC2021 (**2021**) 359.

[26] J. Glombitza on behalf of the Pierre Auger Collaboration, Proc. Sci. ICRC2023 (**2023**) 278.
[27] A. Aab *et al.* (Pierre Auger Collaboration), J. Instrum. **16**, P07016 (2021).
[28] A. Abdul Halim *et al.* (Pierre Auger Collaboration), companion paper, Phys. Rev. D **111**, 022003 (2025).
[29] A. Aab *et al.* (The Pierre Auger Collaboration), Nucl. Instrum. Methods Phys. Res., Sect. A **798**, 172 (2015).
[30] H. Kawai *et al.*, Nucl. Phys. B, Proc. Suppl. **175–176**, 221 (2008).
[31] A. Aab *et al.* (Pierre Auger Collaboration), J. Instrum. **15**, P10021 (2020).
[32] J. Abraham *et al.* (Pierre Auger Collaboration), Nucl. Instrum. Methods Phys. Res., Sect. A **613**, 29 (2010).
[33] A. Aab *et al.* (Pierre Auger Collaboration), Phys. Rev. D **90**, 012012 (2014).
[34] M. Ave, M. Roth, and A. Schulz, Astropart. Phys. **88**, 46 (2017).
[35] S. Hochreiter and J. Schmidhuber, Neural Comput. **9**, 1735 (1997).
[36] E. Hoogeboom, J. W. T. Peters, T. S. Cohen, and M. Welling, arXiv:1803.02108.
[37] E. Santos on behalf of the Pierre Auger Observatory, Proc. Sci. ICRC2021 (**2021**) 232.
[38] D. Heck, J. Knapp, J. N. Capdevielle, G. Schatz, and T. Thouw, FZKA **6019** (1998).
[39] R. Sato on behalf of the Pierre Auger Collaboration, in Proceedings of the 32nd ICRC (2011); arXiv:1107.4806.
[40] O. Zapparrata on behalf of the Pierre Auger Collaboration, Proc. Sci. ICRC2023 (**2023**) 266.
[41] A. Aab *et al.* (Pierre Auger Collaboration), Phys. Rev. Lett. **117**, 192001 (2016).
[42] A. Aab *et al.* (Pierre Auger Collaboration), Phys. Rev. Lett. **126**, 152002 (2021).
[43] A. Abdul Halim *et al.* (Pierre Auger Collaboration), Phys. Rev. D **109**, 102001 (2024).
[44] P. Abreu *et al.* (Pierre Auger Collaboration), Phys. Rev. Lett. **109** (2012).
[45] A. Yushkov on behalf of the Pierre Auger Collaboration, Proc. Sci. ICRC2019 (**2019**) 482.
[46] M. de Domenico, M. Settimo, S. Riggi, and E. Bertin, J. Cosmol. Astropart. Phys. 07 (2013) 050.
[47] T. Pierog, I. Karpenko, J. M. Katzy, E. Yatsenko, and K. Werner, Phys. Rev. C **92**, 034906 (2015).
[48] S. Ostapchenko, Nucl. Phys. B, Proc. Suppl. **151**, 143 (2006).
[49] F. Riehn, R. Engel, A. Fedynitch, T. K. Gaisser, and T. Stanev, Phys. Rev. D **102**, 063002 (2020).
[50] T. Fitoussi on behalf of the Pierre Auger Collaboration, Proc. Sci. ICRC2023 (**2023**) 319.
[51] P. Abreu *et al.* (Pierre Auger Collaboration), Eur. Phys. J. C **81** (2021).
[52] M. Unger, G. R. Farrar, and L. A. Anchordoqui, Phys. Rev. D **92**, 123001 (2015).
[53] A. Castellina on behalf of the Pierre Auger Collaboration, EPJ Web Conf. **210**, 06002 (2019).
[54] N. Langner on behalf of the Pierre Auger Collaboration, Proc. Sci. ICRC2023 (**2023**) 371.
[55] S. Hahn on behalf of the Pierre Auger Collaboration, Proc. Sci. ICRC2023 (**2023**) 318.